Model Predictive Control of Three-Level Inverter-Fed Induction Motor Drives with Switching Frequency Reduction

Yongchang Zhang, Yuning Bai
Inverter Technologies Engineering Research Center of Beijing, North China University of Technology, Beijing, China
Email: yozhang@ieee.org

***Abstract*—Model predictive control (MPC) has recently emerged as a powerful control method for ac motor drives, featuring quick dynamic response and intuitive concept. However, conventional MPC requires lots of calculation resources due to the enumeration of each possible voltage vector, especially in the case of a multilevel converter. To achieve good performance with low switching frequency for high power drives, the state-of-the-art method uses multi-step prediction, which is even more complicated. This paper proposes a single-vector-based MPC for induction motor (IM) drive supplied by a three-level neutral-point-clamped (3L-NPC) inverter operating at low switching frequency. Instead of torque and flux control in conventional MPC, an equivalent stator flux vector is firstly constructed from the reference value of torque and stator flux, and then the desired voltage vector reference is obtained based on the principle of deadbeat flux control. An optimal cost function is proposed to select the best voltage vector which is closest to the reference voltage vector. Only the voltage vectors producing no more than one jumps in both phase and line voltages are considered as the candidate voltage vectors, which greatly reduces the number of predictions. Furthermore, the suppression of neutral point potential fluctuation and switching frequency limitation are also considered in the cost function. Experimental results are presented to validate the effectiveness of the proposed method at 500 to 760 Hz switching frequency.**

I. Introduction

Compared with the two-level inverter, the 3L-NPC topology is more suitable for high power medium voltage drives because of its lower voltage stress across semiconductor devices and less harmonic distortion in ac side [1]. Different from low power applications, low switching frequency is essential to minimize the switching losses while increasing the utilization of power capability for medium voltage inverters [2]. Unlike two-level inverter, voltage vectors of 3L-NPC can not be switched arbitrarily in practical industrial applications [1]. In other words, smooth vector switching strategy is needed in order to prevent the inverter from being damaged and producing too much harmonics.

Among various control methods, MPC has recently emerged as a powerful control method for high performance closed-loop control of power converters and motor drives, especially in the applications requiring low switching frequency [3]. To apply MPC to 3L-NPC, the neutral point voltage balance and average switching frequency reduction should be taken into account. In [4], a finite-state predictive torque control (PTC) is proposed for 3L-NPC inverter-fed IM drives, which achieves good steady state and dynamic performance with the consideration of neutral point voltage balance. However, it requires three weighting factors in the cost function and did not consider the limitation of voltage jumps. The average switching frequency is as high as 1.5 kHz, which is not suitable for high power drives. In [5], a long-horizon prediction is used to achieve better performance than conventional short-horizon prediction while keeping low switching frequency at steady state. Both neutral point voltage and allowed voltage vector jumps are considered. However, it requires lots of calculation resources due to the multi-step prediction, which is computationally intensive and time-consuming, especially in the case of multilevel converter.

To reduce the computational burden of multi-step MPC, sphere decoding is used in [6]. But for long prediction horizons and high sampling frequency, the computation time is still too long. In [7], approximate dynamic programming (ADP) is combined with MPC and the scheme achieves comparable performance to formulations with long prediction horizons. In [8], a strategy combines MPC with selective harmonic elimination pulse width modulation (SHE-PWM) is proposed. Not only a fast dynamic response is obtained, but also a predefined voltage and current spectrum with low switching frequency is achieved in steady state. The main disadvantage of the methods described above is that the neutral point voltage balance is not considered. In other words, these methods require a fixed neutral point potential.

This paper tries to develop a low complexity MPC with short horizon prediction for 3L-NPC inverter-fed IM drives operating at low switching frequency. Different from prior methods [4], [5], [9] using torque and stator flux as control variables, the proposed method firstly obtains an equivalent stator flux vector from the reference value of torque and stator flux [10]. A reference voltage vector nullifying the stator flux error at the end of next control period is calculated from the stator voltage equation. A carefully designed cost function is proposed, which considers the voltage vector error, the suppression of neutral point potential fluctuation and switching frequency reduction. The required predictions are no more than 7 at most by considering the voltage vectors producing no more than one jumps in both phase and line voltages, which not only reduces the computational burden but is also beneficial to switching frequency reduction. The proposed

978-1-5386-1127-2/17/$31.00 ©2017 IEEE

method achieved good performance with only 500 to 760 Hz switching frequency and its effectiveness is confirmed by the test results from a low voltage 3L-NPC inverter-fed IM drive.

II. Model of IM and 3L-NPC Inverter

A. Dynamic Model of IM

When stator current $\boldsymbol{i}_s$ and stator flux $\boldsymbol{\psi}_s$ are chosen as state variables in a stationary reference frame, the state-space model of IM can be described by:

$$\frac{d\boldsymbol{x}}{dt} = \boldsymbol{A}\boldsymbol{x} + \boldsymbol{B}\boldsymbol{u} \tag{1}$$

where $\boldsymbol{x} = \begin{bmatrix} \boldsymbol{i}_s & \boldsymbol{\psi}_s \end{bmatrix}^T$ are state variables; $\boldsymbol{u} = \boldsymbol{u}_s$ is the stator voltage vector and

$$\boldsymbol{A} = \begin{bmatrix} -\lambda(R_s L_r + R_r L_s) + j\omega_r & \lambda(R_r - jL_r\omega_r) \\ -R_s & 0 \end{bmatrix}$$

$$\boldsymbol{B} = \begin{bmatrix} \lambda L_r \\ 1 \end{bmatrix}$$

where R_s, R_r, L_s, L_r and L_m are the stator resistance, rotor resistance, stator inductance, rotor inductance and mutual inductance, respectively; ω_r is electrical rotor speed and $\lambda = 1/\left(L_s L_r - L_m^2\right)$.

In this paper, the Heun's method [10] is used to discretize (1) for higher accuracy, which is expressed as:

$$\begin{cases} \boldsymbol{x}_p^{k+1} &= \boldsymbol{x}^k + T_{sc}(\boldsymbol{A}\boldsymbol{x}^k + \boldsymbol{B}\boldsymbol{u}_s^k) \\ \boldsymbol{x}^{k+1} &= \boldsymbol{x}_p^{k+1} + \frac{T_{sc}}{2}\boldsymbol{A}(\boldsymbol{x}_p^{k+1} - \boldsymbol{x}^k) \end{cases} \tag{2}$$

where T_{sc} is control period, $\boldsymbol{x}_p^{k+1}$ is predictor-corrector of state vector; $\boldsymbol{x}^{k+1} = \begin{bmatrix} \boldsymbol{i}_s^{k+1} & \boldsymbol{\psi}_s^{k+1} \end{bmatrix}^T$ is predicted vector of stator current and stator flux at $(k+1)$th instant.

The rotor flux at $(k+1)$th instant can be computed based on stator flux $\boldsymbol{\psi}_s^{k+1}$ and current $\boldsymbol{i}_s^{k+1}$ as:

$$\boldsymbol{\psi}_r^{k+1} = \frac{L_r}{L_m}\boldsymbol{\psi}_s^{k+1} - \frac{1}{\lambda L_m}\boldsymbol{i}_s^{k+1}, \tag{3}$$

and the electromagnetic torque can be predicted as [11]:

$$T_e^{k+1} = \frac{3}{2}N_p\lambda L_m(\boldsymbol{\psi}_r^{k+1} \otimes \boldsymbol{\psi}_s^{k+1}). \tag{4}$$

where N_p is the number of pole pairs and $\otimes$ represents cross product of two vectors.

B. Model of 3L-NPC Inverter

The circuit topology of the induction motor drive fed by a 3L-NPC inverter is shown in Fig. 1. With different switching states S_a^k, S_b^k, S_c^k, each phase of the motor can be connected to either the positive (p), negative (n), or neutral (o) point of the dc-link. In this paper, switching states are labeled as '2', '0', '1' for 'p', 'n', 'o' respectively. As shown in Fig. 2, the inverter produces 27 voltage vectors in four categories: large voltage vectors (LVV), medium voltage vectors (MVV), small voltage vectors (SVV) and zero voltage vectors (ZVV).

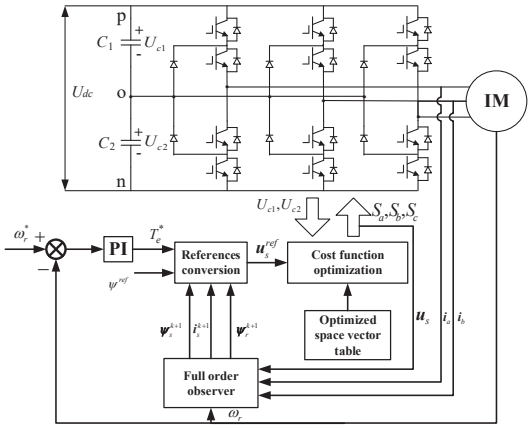

Fig. 1. Circuit topology and control diagram of the proposed MPC

The deviation of the neutral point voltage is defined as the difference between the upper capacitor voltage and the lower capacitor voltage in the dc-link:

$$\triangle U_{mid} = U_{c1} - U_{c2}. \tag{5}$$

The capacitor voltages are charged or discharged only by MVVs and SVVs while LVVs and ZVVs have no effect on $\triangle U_{mid}$ [12]. It should be noted that there are a pair of SVVs producing the same line voltage, but their influences on neutral point voltage are opposite [13]. $\triangle U_{mid}$ at $(k+1)$th instant is given as follows [14]:

$$\triangle U_{mid}^{k+1} = \frac{T_{sc}}{C}\begin{bmatrix} \left|S_a^k - 1\right| & \left|S_b^k - 1\right| & \left|S_c^k - 1\right| \end{bmatrix}\begin{bmatrix} i_a^k \\ i_b^k \\ i_c^k \end{bmatrix} + \triangle U_{mid}^k, \tag{6}$$

where i_a^k, i_b^k and i_c^k are three phases current at kth instant; $C = C_1 = C_2$ is the dc-link capacitor, as shown in Fig. 1. By applying suitable voltage vectors, the average value of $\triangle U_{mid}$ can be maintained around zero.

III. Principle of the Proposed MPC

The overall control diagram of the proposed MPC is shown in Fig. 1, which is mainly composed of the following parts: full order observer, reference conversion, cost function optimization and optimized space vector table. The torque command is obtained through an external speed control loop using PI controller. The stator flux amplitude is kept constant because the flux-weaken operation is not considered in this paper. The detailed introduction of the other parts in the control diagram will be elaborated in the following text.

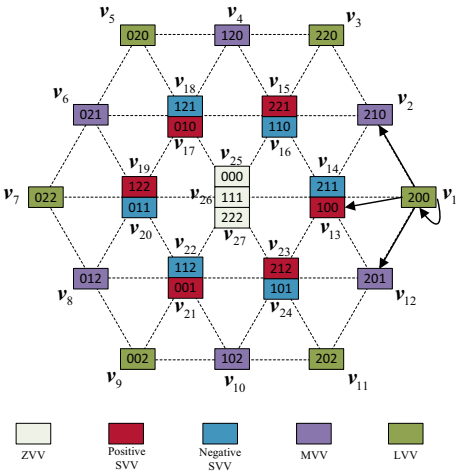

Fig. 2. Space vector graph of 3L-NPC inverter

A. Estimation and Prediction of Stator Flux

Accurate state estimation is a key factor to achieve a good performance of MPC in real implementation. A closed-loop full order observer is adopted in this paper [10]. By introducing the error feedback of stator current, the accuracy of estimation is improved. The mathematical model of the observer is shown as:

$$\frac{d\hat{\boldsymbol{x}}}{dt} = \boldsymbol{A}\hat{\boldsymbol{x}} + \boldsymbol{B}\boldsymbol{u}_s + \boldsymbol{G}(\boldsymbol{i}_s - \hat{\boldsymbol{i}}_s), \tag{7}$$

where $\hat{\boldsymbol{x}} = \begin{bmatrix} \hat{\boldsymbol{i}}_s & \hat{\boldsymbol{\psi}}_s \end{bmatrix}^T$ are state variables representing the estimated stator current and stator flux.

To reduce computational burden and improve stability of the observer, a constant gain matrix $\boldsymbol{G}$ is employed as:

$$\boldsymbol{G} = -\begin{bmatrix} 2b \\ b/(\lambda L_r) \end{bmatrix}, \tag{8}$$

where b is a negative constant. Normally, b needs to be adjusted by trial and error and $b = -40$ is used in this paper. In digital implementation, the observer is discretized using Heun's method introduced in Section II-A.

B. Voltage Reference Calculation

In this paper, the torque reference T_e^{ref} and the stator flux amplitude reference ψ^{ref} are replaced by a new stator flux vector reference $\boldsymbol{\psi}_s^{ref}$ equivalently. The magnitude of stator flux vector reference $\boldsymbol{\psi}_s^{ref}$ is set to a constant value ψ^{ref} when the machine runs below the rated speed, namely that:

$$|\boldsymbol{\psi}_s^{ref}| = \psi^{ref}. \tag{9}$$

The torque can be expressed as a cross product of stator flux and rotor flux, which is shown as (4). Meanwhile, the rotor flux $\boldsymbol{\psi}_r$ is estimated by (3). According to (4), the references of T_e^{ref} and ψ^{ref} should satisfy the following equations:

$$\boldsymbol{\psi}_s^{ref} = \psi_s^{ref} \exp(j \cdot \angle \boldsymbol{\psi}_s^{ref}), \tag{10}$$

$$\angle \boldsymbol{\psi}_s^{ref} = \angle \boldsymbol{\psi}_r + \arcsin\left(\frac{T_e^{ref}}{\frac{3}{2}N_p \lambda L_m |\boldsymbol{\psi}_r| \psi^{ref}}\right). \tag{11}$$

Based on (4), (10) and (11), the new stator flux vector reference $\boldsymbol{\psi}_s^{ref}$ is transferred from the reference T_e^{ref} and ψ^{ref}. To achieve deadbeat control of $\boldsymbol{\psi}_s^{ref}$, the stator voltage vector reference in stationary frame can be obtained from (1) as:

$$\boldsymbol{u}_s^{ref} = R_s \boldsymbol{i}_s^{k+1} + \frac{\boldsymbol{\psi}_s^{ref} - \boldsymbol{\psi}_s^{k+1}}{T_{sc}}. \tag{12}$$

Obviously, if $\boldsymbol{u}_s^{ref}$ is traced quickly and accurately, T_e^{ref} and ψ^{ref} will be satisfactorily controlled.

C. Cost Function Minimization

MPC is very flexible and powerful in handling multiple control objectives. For IM drive fed by a 3L-NPC inverter, the main aim is to minimize the tracking error of torque and flux linkage. Furthermore, neutral point voltage error should be minimized and switching frequency should be reduced. Finally, no more than one switching jump is permitted between the applied voltage vector and the last voltage vector. The first two aims can be satisfied by minimizing the following cost function based on (6) and (12):

$$J_1 = \left|\boldsymbol{u}_s^{ref} - \boldsymbol{v}^k\right| + K_{mid}\left|\triangle U_{mid}^{k+1}\right|^2 + K_n n_{sw} \tag{13}$$

where $\boldsymbol{v}^k$ is the output voltage vector of 3L-NPC inverter, which is defined by applied switching states S_a^k, S_b^k, S_c^k; $n_{sw}$is the number of switching transitions and can be calculated by the last switching states S_a^{k-1}, S_b^{k-1}, S_c^{k-1}:

$$n_{sw} = \sum_{x=\{a,b,c\}} \left|S_x^k - S_x^{k-1}\right|; \tag{14}$$

K_{mid} and K_n denote the weighting factors for neutral point voltage balance and average switching frequency, respectively. By adjusting K_{mid} and K_n, the impact of the neutral point voltage balance control and average switching frequency reduction can be weakened or enhanced as desired.

Different from the classical cost function consisting of three weighting factors, shown in (15), the new cost function (13) removes the factor for stator flux k_ψ [9]. In other words, tuning work is slightly reduced. Meanwhile, a square constraint is used to balance the neutral point voltage fluctuation, which has a stronger binding force.

$$J_2 = \left|T_e^{ref} - T_e\right| + k_\psi \left|\psi^{ref} - |\boldsymbol{\psi}_s|\right| + K_{mid}\left|\triangle U_{mid}^{k+1}\right|^2 + K_n n_{sw} \tag{15}$$

TABLE I
PARTIAL SWITCHING TABLE

Categories	Voltage vector	Candidate vectors
LVV	$\boldsymbol{v}_1$	$\boldsymbol{v}_1$, $\boldsymbol{v}_2$, $\boldsymbol{v}_{12}$, $\boldsymbol{v}_{13}$
MVV	$\boldsymbol{v}_2$	$\boldsymbol{v}_1$, $\boldsymbol{v}_2$, $\boldsymbol{v}_3$, $\boldsymbol{v}_{14}$,$\boldsymbol{v}_{16}$
SVV	$\boldsymbol{v}_{13}$	$\boldsymbol{v}_1$, $\boldsymbol{v}_{13}$, $\boldsymbol{v}_{16}$, $\boldsymbol{v}_{24}$, $\boldsymbol{v}_{25}$
ZVV	$\boldsymbol{v}_{26}$	$\boldsymbol{v}_{14}$, $\boldsymbol{v}_{16}$, $\boldsymbol{v}_{18}$, $\boldsymbol{v}_{20}$, $\boldsymbol{v}_{22}$, $\boldsymbol{v}_{24}$, $\boldsymbol{v}_{26}$

TABLE II
MACHINE AND CONTROL PARAMETERS

DC-bus voltage	U_{dc}	540 V
Rated power	P_N	2.2 kW
Rated voltage	U_N	380 V
Rated frequency	f_N	50 Hz
Rated torque	T_N	14 Nm
Number of pole pairs	N_p	2
Stator resistance	R_s	3.065 Ω
Rotor resistance	R_r	1.879 Ω
Mutual inductance	L_m	0.232 H
Stator inductance	L_s	0.242 H
Rotor inductance	L_r	0.242 H
Flux amplitude reference	ψ^{ref}	0.9 Wb
DC-link capacitors	C_1, C_2	2240μF

D. Optimized Space Vector Table

It should be noted that, the voltage jump is not explicitly considered in the cost function (13). In fact, this problem is solved when selecting the candidate voltages to be evaluated in (13). For example, if the selected optimal voltage vector in the last control period is $\boldsymbol{v}_1$, the candidate vectors needed to be evaluated are only the neighboring vectors, namely $\boldsymbol{v}_1$, $\boldsymbol{v}_2$, $\boldsymbol{v}_{12}$ and $\boldsymbol{v}_{14}$, as shown in Fig. 2. In other words, the rest of voltage vectors producing excessive voltage jumps or more than one switching jump are ruled out directly. To clarify the vector switching strategy, a example of switching table is given in table I. As shown in table I, the candidate vectors contain the current state itself. In other words, the value of n_{sw} mentioned in (14) is 0 or 1.

Based on this strategy, smooth vector switching is achieved. And only 4 (for LVVs) to 7 (for $\boldsymbol{v}_{26}$) voltage predictions are needed in proposed MPC, instead of 27 torque and flux predictions in traditional method. Hence, the proposed strategy is more efficient.

IV. EXPERIMENTAL RESULTS

To confirm the effectiveness of the proposed MPC, experimental tests are carried out on a 3L-NPC inverter-fed IM drive. The motor parameter is same as the table II. And a 32bit floating point DSP TMS320F28335 is utilized to execute the main control algorithm with 10 kHz sampling frequency. The experimental data are obtained from a Scope Coder DL850 and transferred to PC for analysis. The curves shown in flowing oscillograms are rotor speed ω_r, electromagnetic torque T_e , stator flux amplitude ψ_s, the deviation of the neutral point voltage $\triangle U_{mid}$ defined in (5) and one-phase stator current i_a.

Fig. 3a presents the starting responses from standstill to 1500 rpm for the proposed method. Before the system starts, the neutral point potential is not zero because the capacitance

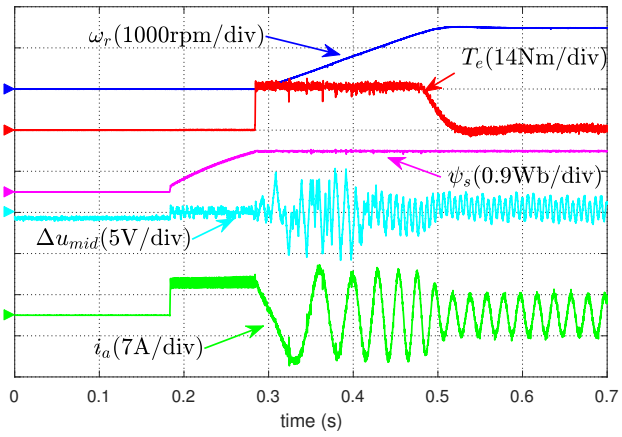

(a)

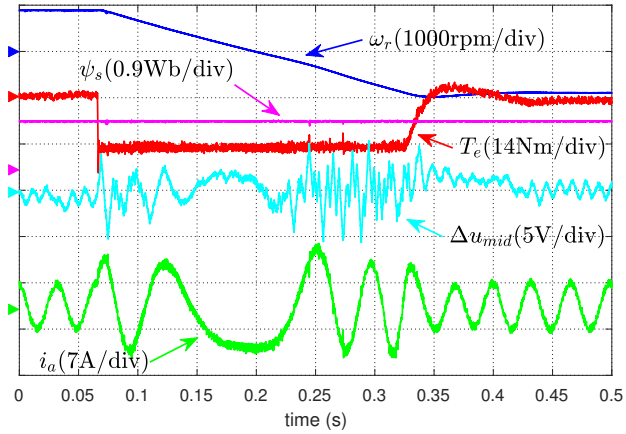

(b)

Fig. 3. Experimental dynamic response of the proposed MPC, (a) starting from standstill to 1500 rpm, (b) responses of speed reversal at ± 900 rpm.

in the experimental device has a slight parameter difference. In order to avoid large starting current while providing sufficient starting torque, the stator flux is firstly established by the current chopping control. It is seen that the motor accelerates quickly to 1500 r/min while the peak current is limited within 10A (less than 1.5 times nominal value). At the same time, even in the large dynamic process, the neutral point voltage fluctuation is also suppressed to some extent.

Furthermore, the speed reversal experiment from 900 rpm to -900 rpm is presented in Fig. 3b. The tested results show that the motor decelerates quickly to zero speed and then accelerates fast to the target speed. Meanwhile, it is clearly seen that the stator flux is almost constant, illustrating that the decoupled control of stator flux and torque can be realized.

Apart from dynamic responses, the steady state tests at low and high speeds with rated load are also presented. As shown in Fig. 4, similar to the dynamic case, the neutral point voltage $\triangle U_{mid}$ is limited within 5V, which is about 1% of DC bus voltage (540V). For Fig. 4b, the average switching frequency is only about 520 Hz. The line voltage waveform of this condition is shown in Fig. 5. It can be seen that no excessive

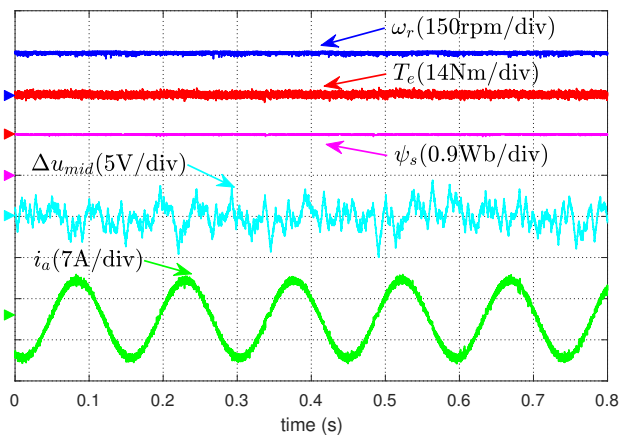

(a)

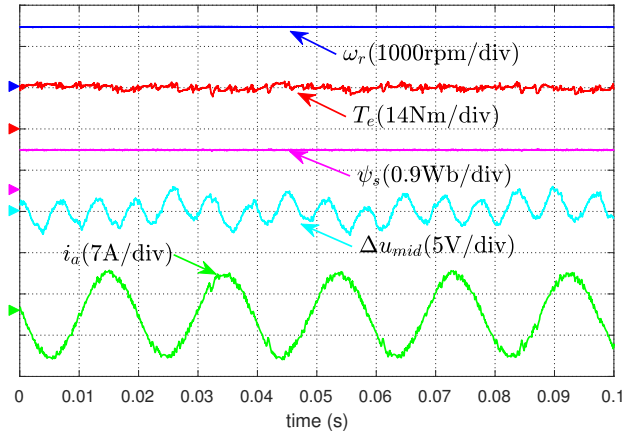

(b)

Fig. 4. Experimental results, (a) low speed operation of 150 rpm with rated load, (b) high speed operation of 1500 rpm with rated load.

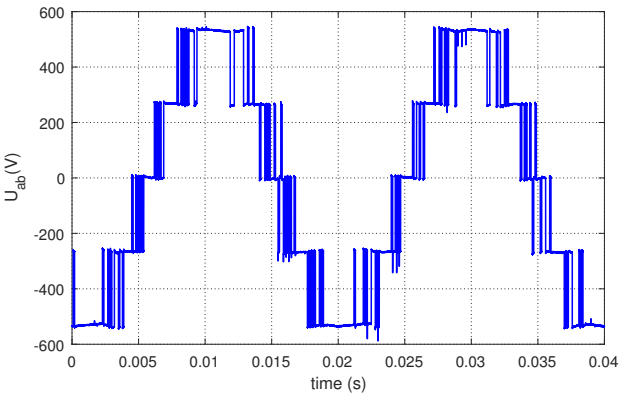

Fig. 5. Experimental line voltage wave when motor is in high speed operation of 1500 rpm with rated load.

voltage jump occurred. Meanwhile, due to the weighting factor K_n in the cost function, the average switching frequency is reduced. In a period of time, switches remain in their original state without action, through which the switching losses are reduced.

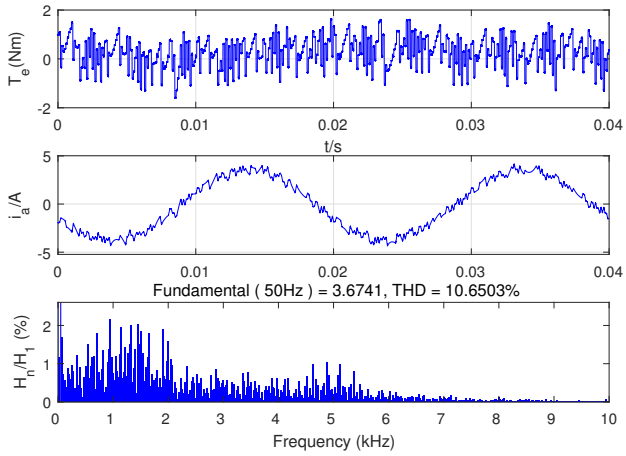

Fig. 6. Experimental high speed operation of 1500 rpm without load.

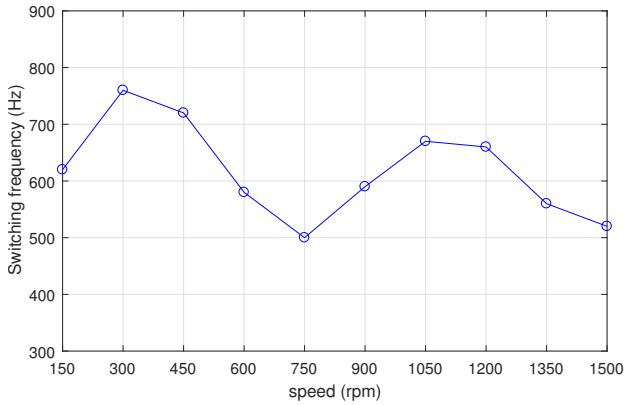

Fig. 7. Average switching frequencies at different speeds with rated load for the proposed method.

Finally, the average switching frequencies at various speeds with rated load are exhibited in Fig. 7. The average switching frequency f_{av} is obtained by counting the total switching actions N of twelve semiconductors of three-level inverter over a fixed period of 1s, namely that $f_{av} = N/12$. At 300 revolutions per minute (rpm) the average switching frequency is 760 Hz, while at 750 rpm the frequency is 500 Hz. The curve in Fig. 7 shows the shape of M, which is quite different from curves of two-level inverter [15]. The reason is that SVVs are often used during mid speed region and the tendency to change voltage vectors is suppressed by the cost function. Same phenomenon can also be observed in the high speed region, where MVVs and LVVs are used, as shown in Fig. 5.

V. Conclusion

This paper proposes an effective MPC method for 3L-NPC inverter-fed IM drives with switching frequency reduction. The reference voltage vector is firstly calculated based on the principle of deadbeat flux control, which serves as the main control variable to be tracked. The suppression of neutral point potential fluctuation and switching frequency reduction are considered in the cost function. Only appropriate voltage vec-

tors satisfying the requirements of voltage jumps are evaluated in the cost function, which significantly reduces the required predictions and computational burden. The proposed method is experimentally tested on a low voltage 3L-NPC inverter-fed IM drive, which shows good steady state performance and quick dynamic response with low switching frequency of 500 Hz to 760 Hz. The experimental results confirm the effectiveness of the proposed MPC.

ACKNOWLEDGMENT

This work was supported in part by the National Natural Science Foundation of China under Grant 51577003, and in part by the Beijing Natural Science Foundation under Grant 3162012.

REFERENCES

[1] Y. Zhang, J. Zhu, Z. Zhao, W. Xu, and D. G. Dorrell, "An improved direct torque control for three-level inverter-fed induction motor sensorless drive," *IEEE Trans. Power Electron.*, vol. 27, no. 3, pp. 1502–1513, Mar. 2012.

[2] J. Holtz, "Advanced PWM and predictive control —an overview," *IEEE Trans. Ind. Electron.*, vol. 63, no. 6, pp. 3837–3844, Jun. 2016.

[3] S. Vazquez, J. Rodriguez, M. Rivera, L. G. Franquelo, and M. Norambuena, "Model predictive control for power converters and drives: Advances and trends," *IEEE Trans. Ind. Electron.*, vol. 64, no. 2, pp. 935–947, Feb. 2017.

[4] M. Habibullah, D. D. C. Lu, D. Xiao, and M. F. Rahman, "Finite-state predictive torque control of induction motor supplied from a three-level npc voltage source inverter," *IEEE Trans. Power Electron.*, vol. 32, no. 1, pp. 479–489, Jan. 2017.

[5] T. Geyer and D. E. Quevedo, "Performance of multistep finite control set model predictive control for power electronics," *IEEE Trans. Power Electron.*, vol. 30, no. 3, pp. 1633–1644, Mar. 2015.

[6] R. Baidya, R. Aguilera, P. Acuna, S. Vazquez, and H. D. Mouton, "Multistep model predictive control for cascaded h-bridge inverters: Formulation and analysis," *IEEE Trans. Power Electron.*, vol. PP, no. 99, pp. 1–1, 2017.

[7] B. Stellato, T. Geyer, and P. J. Goulart, "High-speed finite control set model predictive control for power electronics," *IEEE Trans. Power Electron.*, vol. 32, no. 5, pp. 4007–4020, May 2017.

[8] R. P. Aguilera, P. Acuña, P. Lezana, G. Konstantinou, B. Wu, S. Bernet, and V. G. Agelidis, "Selective harmonic elimination model predictive control for multilevel power converters," *IEEE Trans. Power Electron.*, vol. 32, no. 3, pp. 2416–2426, March 2017.

[9] M. HABIBULLAH, D. D. C. Lu, D. Xiao, I. Osman, and M. Rahman, "Selected prediction vectors based fs-ptc for 3l-npc inverter fed motor drives," *IEEE Trans. Ind. Appl.*, vol. PP, no. 99, p. 1, 2017.

[10] Y. Zhang and H. Yang, "Two-vector-based model predictive torque control without weighting factors for induction motor drives," *IEEE Trans. Power Electron.*, vol. 31, no. 2, pp. 1381–1390, Feb. 2016.

[11] ——, "Model-predictive flux control of induction motor drives with switching instant optimization," *IEEE Trans. Energy Convers.*, vol. 30, no. 3, pp. 1113–1122, Sep. 2015.

[12] J. Pou, R. Pindado, D. Boroyevich, and P. Rodriguez, "Evaluation of the low-frequency neutral-point voltage oscillations in the three-level inverter," *IEEE Trans. Ind. Electron.*, vol. 52, no. 6, pp. 1582–1588, Dec. 2005.

[13] N. Celanovic and D. Boroyevich, "A comprehensive study of neutral-point voltage balancing problem in three-level neutral-point-clamped voltage source PWM inverters," *IEEE Trans. Power Electron.*, vol. 15, no. 2, pp. 242–249, Mar. 2000.

[14] Y. Zhang, Y. Peng, and J. Zhu, "Efficient model predictive power control for three-level AC/DC converters," in *Proc. 18th Int. Conf. Electrical Machines and Systems (ICEMS)*, Oct. 2015, pp. 2127–2133.

[15] Y. Zhang, H. Yang, and B. Xia, "Model-predictive control of induction motor drives: Torque control versus flux control," *IEEE Trans. Ind. Appl.*, vol. 52, no. 5, pp. 4050–4060, Sep. 2016.